Contributions of climate change and groundwater extraction to soil moisture trends

Longhuan Wang[1,2], Zhenghui Xie[1*], Binghao Jia[1], Jinbo Xie[1], Yan Wang[1,2], Bin Liu[1,2], Ruichao Li[1,2], Si Chen[1,2]

[1]State Key Laboratory of Numerical Modeling for Atmospheric Sciences and Geophysical Fluid Dynamics, Institute of Atmospheric Physics, Chinese Academy of Sciences, Beijing 100029, China

[2]College of Earth Science, University of Chinese Academy of Sciences, Beijing 100049, China

Correspondence to: Zhenghui Xie (zxie@lasg.iap.ac.cn)

Abstract. Climate change affects water availability for soil, and groundwater extraction influences water redistribution by altering water demand, both of which significantly affect soil moisture. Quantifying their relative contribution to the changes in soil moisture will further our understanding of the mechanisms underlying the global water cycle. In this study, two groups of simulations were conducted with and without groundwater (GW) extraction (estimated based on local water supply and demand) from 1979–2010 using the land surface model CAS-LSM with four global meteorological forcing datasets (GSWP3, PRINCETON, CRU-NCEP, and WFDEI). To investigate the contribution of climate change and GW extraction, a trajectory-based method was used. Comparing the simulated results with the in-situ dataset of the International Soil Moisture Network (ISMN) and the satellite-based soil moisture product of the European Space Agency's Climate Change Initiative (ESA-CCI) indicated that the CAS-LSM reasonably reproduced the distribution of soil moisture, and well matched the temporal changes. Globally, our results suggested a significant decreasing trend in surface soil moisture (0-10cm, 0.98 e−4 $mm^3\ mm^{-3}\ yr^{-1}$) over the 32-year period tested. The drying trends were mainly observed in arid regions such as the tropical desert regions in North Africa and the Arabian Peninsula. While the wetting trends were primarily in tropical forested areas in South America and Northeast Asia. Climate change contributed 101.2% and 90.7% to global drying and wetting trends of surface soil moisture, respectively, while GW extraction accounted for −1.2% and 9.3%, respectively. In deep soil, GW extraction contributed 1.37% and −3.21% to the drying and wetting trends, respectively. The weak influence of GW extraction may be because this activity occurs in limited areas. GW extraction contributed more than 35%

to the change in surface soil moisture in wetting areas where GW overexploitation occurs. GW is mainly extracted for irrigation to alleviate soil water stress in semiarid regions that receive limited precipitation, thereby slowing the drying trend and accelerating the wetting trend of surface soil. However, GW exploitation weakens the hydraulic connection between soil and aquifer, leading to deeper soils drying up. Overall, climate change dominated the soil moisture trends, but the effect of GW extraction cannot be ignored.

1. Introduction

Soil moisture plays a critical role in controlling the exchange of water, energy, and carbon between the land–vegetation–water–atmosphere system (Seneviratne et al., 2010; van den Hurk et al., 2011). Soil drying could increase the possibility of agricultural drought and fire (Dai et al., 2011), and affects plant transpiration, photosynthesis, microbial activity, and a number of biogeochemical processes. Significant decreasing trends in soil moisture can lead to water scarcity, threatening water supply and associated food production (Döll et al., 2009; Wisser et al., 2010; Albergel et al., 2012; Wada et al., 2013; Dai, 2013; Zhan et al., 2016). Soil moisture trends are affected by both climate (e.g., precipitation and temperature) and human activities (e.g., groundwater (GW) extraction). Climate change can affect water availability for soil (Dai, 2013; Wentz et al., 2007; Feng, 2016), and human activities influence the soil water content through altering the surface water flux of soil (Min et al., 2011; Douville et al., 2013; Feng, 2016). GW extraction, such as for irrigation, also has been shown to affect local soil moisture. However, it remains unclear which of these factors exerts more influence owing to the complex interactions involved. Therefore, quantifying the contribution of climate change and GW extraction to soil moisture trends will improve our understanding of how human activities affect soil water content and will help to determine the mechanisms underlying the global water cycle.

Traditionally, trends in soil moisture have been studied using ground-based observations (Robock et al., 2005), which provide a direct record of soil moisture and are used as reference measurements for calibrating other methods for measuring soil moisture (Yin et al., 2018). Since they are limited in space, require significant manpower for sampling (Seneviratne et al., 2010), and cannot always represent larger

scales, remote sensing methods (e.g., passive and active microwave remote sensing) that provide global coverage and excellent temporal sampling of soil moisture are widely used (Albergel et al., 2013). Nevertheless, the accuracy of these measurements depends on the retrieval approach strongly, and determining the contribution of climate and human activities is not easy. As a result, recent studies have mostly relied on model estimates (Wei et al., 2008; Zhan et al., 2016).

Land surface models (LSMs) can be used to calculate soil moisture trends at regional or global scales (Li et al.,2011; Jia et al., 2018). Different LSMs have been developed to simulate soil moisture as a function of meteorological input variables and soil and vegetation parameters over a few decades (e.g., Kowalczyk et al., 2006; Lawrence et al., 2011; Best et al., 2011). Much previous research has focused on the effect of climate change on soil moisture using comprehensive LSMs forced with realistic forcing data (Berg et al., 2003; Guo et al., 2006; Wei et al., 2008; Wang and Zeng, 2011). For the global average, precipitation had a dominant effect on the variability of soil moisture at interannual to decadal time scales; however, temperature was the main cause of the long-term trend in soil moisture. Increased soil drying in the transitional regions was primarily caused by global warming, which is illustrated by regression analysis and LSMs (Cheng and Huang, 2016). Since 1950, rising temperatures have contributed 45% to of the total soil moisture reduction (Cai et al., 2009). In semiarid regions, precipitation and temperature are equally important to the simulations of soil hydrological variables (Wang and Zeng, 2011). Jia et al. (2018) found that precipitation controlled the direction of soil moisture changes using remote sensing data ESA-CCI and modeling of soil moisture by Community Land Model 4.5(CLM4.5) in China. Recently, researchers have focused on incorporating human activity into the hydrological processes of LSMs to assess the influence of anthropogenic activities on hydrological variable simulations. For example, irrigation has been shown to affect soil water content through increased local evapotranspiration and decreased temperatures near the surface (Yu et al., 2014; Zou et al., 2014). GW over-extraction lowers GW tables, reduces total terrestrial water storage, weakens hydraulic connections between aquifers and rivers, and may decrease lake area (Coe and Foley, 2001). Wada et al. (2013) reported that human water consumption is one of the more important mechanisms intensifying hydrological drought. GW exploitation caused drying in deep soil layers and wetting in upper layers, lowering the water table and rapidly reducing terrestrial water storage with severe levels of GW consumption (Zeng et al., 2016a, 2016b, 2017; Xie et al., 2018).

Thus, to our knowledge, the influence of anthropogenic activities (GW extraction) on soil moisture has not been explicitly quantified. Therefore, the main purpose of our study was to assess the relative contribution of GW extraction and climate change to soil moisture trends. To address this issue, the historical land simulations of the Land Surface, Snow and Soil moisture Model Intercomparison Project (LS3MIP) were employed (van den Hurk et al., 2016). Four global meteorological forcing datasets covering the 20th century were used with the land surface model for the Chinese Academy of Sciences (CAS-LSM), which considers human water regulation (HWR) and the movement of frost and thaw fronts (Xie et al., 2018). We compared the simulations with in-situ observations and the ESA CCI satellite-based product to validate the capacity of the CAS-LSM to simulate soil moisture trends. Furthermore, we investigated the interannual variation and trends in simulated soil moisture. Finally, the response of soil moisture temporal variability to climate change and GW extraction was investigated, which can further our understanding of the relationship between soil moisture and climate.

Section 2 discribes the model used in this study, and describes the experimental designs, in-situ observations, and satellite-based data. Then Sect. 3 evaluates the soil moisture simulations in comparison with in-situ observations and satellite-based data. Also, the contributions of climate and GW extraction to soil moisture are discussed, while Sect. 4 outlines our conclusions.

2. Model, data, and experimental design

2.1 Description of CAS-LSM

Xie et al. (2018) incorporated GW lateral flow (GLF), Human Water Regulation (HWR), and the changes in the depth of frost and thaw fronts into CLM4.5 (Oleson, 2013) to develop the high-resolution CAS-LSM. For a detailed description of the physical processes within the CAS-LSM, see Xie et al. (2018). In the present study, only the HWR module was activated. Owing to the coarse resolution (0.9° × 1.25°) of the experiment, it is not possible to describe the water intake of the river, that is, the surface water. Therefore, only GW extraction was considered in our study. Here, only the processes associated with soil water are briefly described below.

The following equation represents the total water balance of the hydrological system:

$$\Delta W_{can} + \Delta W_{sfc} + \Delta W_{sno} + \Delta W_{soil} + \Delta W_a = \left(q_{rain} + q_{sno} + q_s + q_g - ET_{veg,ground,hum} - q_{over} - q_{h2osfc} - q_{drai} - q_{rgwl} - q_{ice}\right)\Delta t \quad \text{Eq. (1)}$$

where the left side denotes the change in canopy water, surface water, snow water, soil water, and ice and water in the unconfined aquifer in turn. q_{rain} is rainfall, q_{sno} is snow, and q_s and q_g represent the rate of surface and GW water use respectively, some of which will return to the soil. q_{over} is surface runoff, q_{h2os} is runoff from surface water storage. q_{rgwl} and q_{ice} are liquid and solid runoff, respectively, from glaciers, wetlands, and lakes. q_{drai} is subsurface drainage and $ET_{veg,ground,huma}$ is evapotranspiration from vegetation, ground, and human water use. Δt is the time step(s).

2.2 Experimental setup

In this study, GSWP3 (Kim et al., 2016), WFDEI (Haddeland et al., 2011; Weedon at al., 2014), CRU-NCEP (Viovy and Ciais, 2009), and PRINCETON (Sheffield et al., 2006) were used to run the offline model. The fields included were air temperature, wind speed, specific humidity, solar radiation, and precipitation. The GSWP3 is based on a dynamical downscaling of the 20th century reanalysis project (Compo et al., 2011), covering the entire 20th century and some of the 21st century (1901–2012) at 0.5° spatial resolution and 3-h intervals. The WATCH forcing data (WFD) are based on the ECMWF-ERA-40 reanalysis data, and were also at 0.5° resolution and 3-h intervals, ceasing in 2001. A subsequent project, EMBARCE, provided the WFDEI, which consisted of 3-h-interval ECMWF ERA-Interim reanalysis data interpolated to 0.5° spatial resolution (1979–2014). Thus, there are offsets for some variables in the overlap period with the WFD. The CRU-NCEP provided 6-h-interval data at 0.5° horizontal spatial resolution (1901–2010). The PRINCETON is based on 6-h-interval surface climate data from the NCEP-NCAR reanalysis. These data are available at 0.5° resolution and 3-h intervals. The version used in this study is from 1901–2012 with a real-time extension based on satellite precipitation and weather model analysis fields. General information about these datasets is summarized in Table 1. Four forcing datasets were bilinearly interpolated to construct a field to a uniform 0.9° × 1.25° to ensure that every simulation had the same soil and vegetation parameters.

We replaced the land cover data with the new generation of "land-use harmonization" (LUH2), which builds on past work from CMIP5 (Hurtt et al., 2011). In addition, monthly irrigation datasets (Zeng et al., 2016b) were used for land model runs, which were developed based on the Food and Agriculture Organization of the United Nations (FAO) global water information system and the Global Map of Irrigation Areas, version 5.0 (GMIA5; Siebert et al., 2005). Industrial and domestic water use were also included and were calculated by the fractions of the total GW water consumption for agricultural,

141 industrial, and domestic water use provided by the FAO. Besides, the changes of the annual GW pumping
142 rate are assumed to vary linearly with population growth and socio-economic development as evidenced
143 by many previous work (Omole 2013; Wu et al. 2014; Zou et al. 2015). The resulting global spatial
144 patterns of GW extraction from 1979 to 2010 is shown in Fig. 2. Notice the GW exploitation hot spots
145 like Europe, southern Iran, the North China Plain, the central United States, northern India and Pakistan
146 are consistent with previous studies (Rodell et al., 2009; Wada et al., 2010).

147 Two sets of numerical experiments were conducted using the default CLM4.5 (hereafter referred to as
148 CTL) and using the CAS-LSM with the HWR module activated (hereafter referred to as NEW). Thus,
149 CTL and NEW contained four simulations, CTL-GSWP3, CTL-CRUNCEP, CTL-PRINCETON, and
150 CTL-WFDEI (prefixed with NEW- for the NEW model). The CTL runs did not include GW extraction,
151 while the NEW runs did include it. Therefore, the difference between the NEW and CTL models would
152 provide a measure of the effect of GW extraction. Simulation spin up followed the TRENDY protocol
153 (http://dgvm.ceh.ac.uk/node/9) by recycling the climate mean and variability from 20 years (1901–1920)
154 of the meteorological forcing. Land use and CO_2 concentration were set to constant at the 1850 level
155 during spin up. All simulations were conducted with horizontal spacing of 0.9° × 1.25°. However, there
156 were differences among the four forcing datasets; therefore, the simulation period covers between 1901
157 and 2010 at a time step of 30 min. Considering that the ESA CCI was available from 1979–2010, our
158 evaluation focused on the same time interval.

159 **2.3 In-situ soil moisture and satellite-based data**

160 To evaluate the capability of the CAS-LSM to simulate soil moisture variation, we retrieved in-situ soil
161 moisture data from the International Soil Moisture Network (ISMN) (Robock et al., 2000; Dorigo et al.,
162 2011; Dorigo et al., 2013). The ISMN is based on in-situ measurements from different regional
163 monitoring projects. For our study, we used data from Africa, Asia, Europe, Australia, and North
164 America networks. Stations with >75% of the observational data missing during the evaluation period
165 were excluded. After which a subset of 225 stations remained (Fig. 2). There were only three dominant
166 contiguous areas in the world (the central USA, the North China Plain, and northern India) with severe
167 levels of GW extraction (Zeng et al., 2016b). Therefore, we focused on validating the ability of the model
168 to accurately represent the soil moisture in these three areas. Further site information is presented in
169 Table 2.

The European Space Agency's Climate Change Initiative (ESA CCI) involves remote sensing projects to monitor global key climate variables with feedback effects on climate change. Soil moisture was then included in 2010. There are three ESA CCI soil moisture products available based on the two types of sensors employed by the project: active microwave remote sensing, passive microwave remote sensing, and a combined product of both active and passive data. The active product was obtained using the SCAT scatterometer and the METOP-A satellite-equipped C-band scatterometer using the algorithm proposed by Wagner et al. (1999). The passive product includes observation data from four satellites, namely the tropical rainfall measuring mission microwave imager, the scanning multichannel microwave radiometer, the specific sensor microwave imager, and the advanced microwave scanning radiometer-Earth observing system. In the present study, we used the combined product (version 3.2), which covers 38 years from 1978–2016 at a daily temporal resolution.

2.4 Analysis method

Taylor's skill score (*S*) (Taylor, 2001) was used to quantitatively evaluate the spatial correlation of modeled soil moisture against the observations with standard deviations as follows:

$$S = \frac{4(1+R)^4}{(\sigma_f + 1/\sigma_f)^2(1+R_0)^4} \quad \text{Eq. (2)}$$

where σ_f is the ratio of the standard deviation of the simulations to the observations, R is the spatial correlation coefficient between the simulation and observation, and R_0 is the maximum possible spatial correlation coefficient. As the model variance approaches the observed variance (i.e., as $\sigma_f \to 1$) and as $R \to R_0$, the skill approaches 1. Thus, a higher value of S indicates a better model performance, and S = 1 when the simulation and observation data are identical.

All simulated datasets were converted to annual means by averaging for the growing season (March–October) before the trend analysis. Precipitation and temperature were treated the same as soil moisture. Trends were calculated using the nonparametric Mann-Kendall test and the Theil-Sen median slope (Sen, 1968) was used to delineate the trends.

To quantify the contribution of the climate and GW extraction to the trends in soil moisture, we used a trajectory method (Feng et al., 2014). The "trajectory" refers to studying the change of GW extraction that occur within a certain period of time for a given grid or region. We can study the effect on soil moisture due to GW extraction in this way. Soil moisture in the CTL experiment represented the effect

198 of climate on soil moisture trends and served as a reference for isolating the contribution of GW
199 extraction. The contributions were calculated with area weight summarization as follows:

200 $$Con_{gw,global} = \frac{R_{gw}(T_{gw} - T_{ctl})}{T} \times 100\% \quad \text{Eq. (3)}$$

201 $$Con_{cm,global} = (1 - Con_{gw,global}) \times 100\% \quad \text{Eq. (4)}$$

202 where $Con_{gw,global}$ and $Con_{cm,global}$ are the global contributions of GW extraction and climate,
203 respectively; R_{gw} is the area ratio of GW extraction in the drying or wetting areas; T_{gw} and T_{ctl} are
204 the drying or wetting soil moisture trends in the GW and non-GW extraction regions, respectively; and
205 T is the soil moisture trend in the global drying or wetting zones.

206 Contributions of climate and GW extraction to certain grids were calculated as follows:

207 $$Con_{gw,grid} = \frac{(T_{gw} - T_{ctl})}{T_{gw}} \times 100\% \quad \text{Eq. (5)}$$

208 $$Con_{cm,grid} = (1 - Con_{gw,grid}) \times 100\% \quad \text{Eq. (6)}$$

209 where $Con_{gw,grid}$ and $Con_{cm,grid}$ are the contributions of GW extraction and climate to each grid,
210 respectively; T_{gw} and T_{ctl} are the soil moisture trends at each grid in the NEW and CTL experiments,
211 respectively.

212 **3. Results**

213 **3.1 Validation**

214 First, we compared the spatial distribution of simulated soil moisture with the ESA CCI product. Figure
215 1a, c, e, g shows the linear correlation coefficients between the ESA-CCI and the simulated top-10-cm
216 soil moisture from 1979-2010. The top-10-cm soil moisture is a weighted average of the first four soil
217 layer thicknesses (1.75, 2.76, 4.55, and 7.5 cm; the weights are 0.175, 0.276, 0.455, and 0.094,
218 respectively). The correlations between the simulated and ESA CCI data were significantly positive in
219 most areas ($r > 0.6$). Modeled results were more accurate in humid and temperature zones especially in
220 India and Southeast Asia ($r > 0.9$). Results revealed that the interannual variability of soil moisture cannot
221 be well captured in northern high-latitude areas (no correlation or negative correlations). This is partly
222 due to the limited ability of remote sensing technique in detecting soil moisture in frozen soils or under
223 snow cover.

Figure 1b, d, f, h shows the differences between NEW-simulations and ESA CCI data. Soil moisture from all forcing datasets presented similar broad patterns. ESA-CCI had lower soil moisture compared with the simulated results from Europe and the eastern USA. While Fig. 1f shows the results from CRU-NCEP are drier than those from the other three at high latitudes in the northern hemisphere. The simulation results in WFD were wetter overall, and the PRINCETON drier in South America and Central Africa. However, overall, the results from PRINCETON and GSWP3 simulation were closer. Soil moisture from NEW was 0.06% to 0.09% higher than that from CTL. The area represented by NEW is irrigated; thus, the top 10 cm of soil is wetter in NEW than in CTL. However, the increase in soil moisture was slight (about 0.001 to 0.2 $mm^3\ mm^{-3}$). The differences between NEW and CTL indicate that GW extraction caused a significant increase in top-10-cm soil moisture in the central USA, the North China Plain, and North India. The three areas with severe levels of GW extraction (Fig. 2).

Figure 3 presents Taylor diagrams comparing the four NEW experiments with the in-situ ISMN observations over the eight subregions (see Table 2 for site details). Figure 3 clearly shows that the model can generally capture the changes in soil moisture in these regions (with high correlation and close to 1). However, the performance of the model decreases as the soil depth increases. Results suggest that the standard deviation ratios at most stations in Africa, Australia, Europe, and North America were close to 1, while those for India, Mongolia, China, and Former Soviet Union countries deviated from 1. Moreover, the different forcing datasets did not perform similarly. GSWP performed relatively poorly in deep soil in Europe, while PRINCETON provided a good estimation for Mongolia. CRUNCEP performed poorly in China and Mongolia. In general, GSWP and WFDEI performed well, except for Europe and Mongolia. Three areas (the central USA, North China Plain, and northern India) with severe levels of GW exploitation were used as key areas for validation. The ground observations of soil moisture in the three regions were retrieved from the ISMN. The usable stations were as follows: seven sites on the North China Plain from 1981–1999, 15 sites in Colorado of central US from 2003–2010, and one site in Kanpur of northern India from 2011–2012. The regional soil moisture from observations and simulations were averaged from all stations and corresponding grid points. Before the comparison, hourly values from all stations were converted into a monthly time series. The soil layer depths in the CAS-LSM did not match those from the ground observations, and the depths of soil moisture observations varied among the three regions. Therefore, we used different methods to match the soil depth of observations to the corresponding soil layer of simulations for the different areas (Table 2).

We evaluated the performance of each forcing dataset over the three regions using Taylor's skill scores, as shown in Fig. 4 (left panel). As Fig. 4a shows, the individual forcing datasets show a varying ability to capture the soil moisture distribution. In the 0–10 cm soil layer, WFD performed well and had the highest skill scores (S = 0.86). Generally, all meteorological forcing datasets performed consistently well for the North China Plain in both the near-surface and deeper soil layers. Performance was also evaluated using a Taylor diagram as shown in Fig. 4d–f. GSWP captured the temporal variability of observed soil moisture with higher correlations than the other datasets. Correlations tended to cluster around 0.7, with the exception of CRUNCEP. Then, the correlations between observations and simulations decreased with soil depth. The radial distance from the origin represents the standard deviation of simulations relative to the standard deviation of observations. CRU-NCEP exhibited much higher ($\sigma_{sim}/\sigma_{obs}$ >1) variation than that of the in-situ observations.

In the central US, WFD performed better with a higher skill score, and CRU-NCEP had the lowest score. Correlations between the simulated 5-cm soil moisture and observations (Fig. 4e) were all lower than 0.5. This may be because the offline runs do not consider the strong interaction between land and atmosphere. All simulations resulted in lower standard deviations than those for observations at 50 cm soil depth. This indicates that the true variability in soil moisture cannot be well reconstructed in this layer using the four forcing datasets tested herein. Errors were also associated with the varying degrees of mismatch between the soil layers of the observations and the model.

Owing to the limitations of the observational data in Kanpur, only three sets of data were compared in that area. Based on the skill scores, WFD and PRINCETON performed well at both 10 cm and 25 cm soil depths, and WFD performed better in deeper soil. The results of a correlation analysis indicated that the simulations from three meteorological forcing datasets (GSWP3, PRINCETON, and WFD) were able to capture the variation in soil moisture (Fig. 4f). Notably, the correlation was higher (>0.9 at North India) when considering the GW extraction, which was not obvious in the other two areas (Fig. 4f). This is because, according to FAO statistics, about 91% of GW extraction was to supply irrigation in India, whereas 64% and 38% of GW extraction was used by agriculture in China and the USA, respectively (Zeng et al., 2016b). Figure 4f shows that the relative standard deviations decreased as soil depth increased, which indicates relatively large errors of fluctuation in the deeper soil layers. Overall, WFDEI provided a better simulation with a higher correlation and a relative standard deviation close to 1.

3.2 Trends in soil moisture

Owing to the uncertainty in meteorological forcing, especially regarding precipitation, which had large differences between different forcing datasets (Table 3), the ensemble average approach was used here. Figure 5 presents the trends in surface soil moisture (0–10 cm), deep soil moisture (200–300 cm), precipitation, temperature, and GW extraction from 1979–2010 from the NEW experiment. Globally, results suggested a significant decreasing trend in surface and deep-soil moisture (−0.98 e−4 and −0.24 e−4 $mm^3\ mm^{-3}\ yr^{-1}$, respectively; $p < 0.05$) over the 32-year period, but the soil moisture trend from PRINCETON was not significant (Table 3). There was a consistent significant warming trend (about 0.016°C yr^{-1}; $p < 0.05$) and a non-significant decreasing precipitation trend ($p > 0.05$). Furthermore, the drying of the surface soil moisture slowed when considering the HWR. The global surface soil moisture decreased at a rate of −0.99 e−4 $mm^3\ mm^{-3}\ yr^{-1}$ without GW extraction. Conversely, the deep soil dried (−0.21 e−4 $mm^3\ mm^{-3}\ yr^{-1}$ in CTL) owing to the rapid lowering of the water table following GW extraction, and the hydraulic connection between the soil and aquifer weakened. More specifically, GW extraction slowed the drying of surface soils in drying areas and increased the wetting trend in wetting areas. The trend in 1.3% of GW extraction areas changed from drying to wetting, with an average GW extraction rate of 171 mm yr^{-1}. The opposite effect was observed in the deeper soil layers.

Figure 6 shows the spatial distribution of soil moisture trends from 1979–2010 obtained from simulations of surface- and deep-soil moisture and ESA CCI. As the depth of the soil increased, the proportion of apparent dryness increased. For the surface soil, the drying trends were mainly found in North Africa, Central Asia, Southwestern USA, Southeast Australia. The wetting trends were primarily in northern South America, northwest Africa, and northeast Asia. This result is consistent with those of previous studies on satellite-based data (Feng, 2015; Dorigo et al., 2012). The trend in the deep soil was consistent with that in the surface layer in most areas, except for Central Asia. Regions with a drying trend always coincided with statistically significant increasing temperature. Many of the strong drying trends occurred over regions that already have relatively low soil moisture. Drying trends were the most prominent in the Sahel in northern Africa. This could be explained by deficits in precipitation during the 1970s and 1980s (Hulme, 1992; L' Hôte et al., 2002). The majority of north Asia exhibited wetting trends with non-significant increasing temperature. Wetting trends were found in the central US, India, and North China Plain, but there were no significant changes.

We further evaluated the ratios of drying/wetting trends for surface and deep soil in different climate regions using the Köppen-Geiger climate classification (Kottek et al., 2006). A brief description of the climate classification is as follows: the first letter refers to the climate types: tropical (A), arid (B), temperate (C), and cold (D). The second letter indicates the precipitation conditions: rainforest (f), monsoon (m), and savannah (s) in tropical and desert (W) and steppe (S) in arid, dry summer (s), dry winter (w), and without dry season (f) in temperate and cold climates. The third letter refers to hot (h) and cold (k) in arid and hot summer (a), warm summer (b), cold summer (c), and very cold summer (d) in temperate and cold climates. At the same time, we used the climate regions defined by Feng et al. (2015), the first climate letter labelled Arid was the arid regions, the second letter "f" was the humid regions and the other regions were the transitional regions. As Figure 7a shows, some arid regions became significantly drier (16.9%) or wetter (9.8%); as did some humid regions (9.8% drier, 9.5% wetter) and transitional regions (12.8% drier, 5.4% wetter). The area of increasing wetness in the Af subregion, which is characterized by tropical rainforests, comprised 22% of its total area. The Dfd subregion is characterized by areas without a dry season and 42.6% of this region rapidly became wetter (about 1.2 e−3 mm^3 mm^{-3} yr^{-1}). Conversely, 21.5% of the BWh subregion, which is characterized by hot deserts, was drying. In the Ds and Dw subregions, which have a hot summer or winter in a year, 30–40% was drying out with a moisture decreasing rate more than −1.2 e−3 mm^3 mm^{-3} yr^{-1}. These results indicate that the drying trends were mainly in arid regions, while the wetting trends were primarily in humid regions. Figure 7b shows that there are proportionally more significant changes in the deeper soil layers. However, the changes are not as great as those in the surface soil. In arid regions (BW and BS subregions), the proportion of apparent drying exceeded 40%. In humid regions (Cfc, Dfc, and Dfd subregions), 30–71% of these areas were significantly wetting. The climatic zone differences in deep soil changes were basically consistent with those in the topsoil, except in Dwc and Dwd regions.

3.3 Contribution of climate change and GW extraction to soil moisture trends

The trend in soil moisture was basically consistent with climate change, but the role of GW extraction was not negligible. Then we quantified the relative contribution of climate and GW intake to the soil moisture trends using the trajectory approach [Eqs. (*2*)–(*3*)]. Results showed that −1.2% of the significant drying trends in the surface soil originated from GW extraction. Thus, the contribution of climate was 101.2%. Regarding the wetting trends, the contribution was 9.3% for GW extraction, with climate

contributing 90.7%. In deep soil, GW extraction contributed 1.37% and −3.21% to the drying and wetting trends, respectively. This indicates that GW extraction only weakly contributes to global wetting and drying trends. This is mainly due to the limited regions of GW extraction. The contribution of GW extraction to surface soil moisture trends is presented in Fig. 8a. In the drying regions, GW extraction and climate change accounted for −19.91% and 119.91%, respectively. Notably, the negative contribution is because that the surface soil moisture is decreasing, while GW extraction slows down the reduction trend (but still decreasing), $T_{gw} - T_{ctl}$ in Eqs. (*5*) is positive, but T_{gw} is negative. In the wetting regions, the contributions were 11.55% and 88.45%, respectively. GW exploitation is mainly used for irrigation to increase moisture in the surface soil, which slows the drying of the surface soil, promoting wetting. Figure 8b shows the contribution of GW extraction in the deeper soil layers. GW extraction positively contributed to the drying trends (109.7%) and negatively contributed to the wetting trends (−5.48%). This indirectly reflects that GW exploitation weakens the hydraulic connection between soil and aquifers. In summary, GW is exploited to provide irrigation, which alleviates water stress in the surface soil, and the deep soil dries due to the loss of hydraulic connection.

As shown in Fig. 8, the contribution of GW extraction mainly occurs in northern Africa, the North China Plain, and central US. Thus, the three regions were selected for further evaluation. Figure 9 further shows the relative contributions to soil moisture trends in three subregions. Contributions of GW extraction to surface soil moisture wetting and drying trends were evident on the North China Plain (drying, up to −62.39%; wetting, 77.74%), northern India (drying, up to −13.56%; wetting, 72.1%), and central US (drying, −57.42%; wetting, 38.51%). For deep soil, the contribution of GW extraction was: North China Plain (drying, 15.12%; wetting, −18.16%), northern India (drying, 56.54%; wetting, 2.07%), and central USA (drying, 23.8%; wetting, −20%). GW extraction can increase the water content of the surface soil, and thus leads to increased moisture in both humid and arid regions. The results revealed that GW extraction contributes more to the soil moisture trends in typical exploitation areas than in the regions without GW extraction. Climate change dominated the soil moisture trends, while the contribution of GW extraction at the regional scale was much greater than that at the global scale, especially in the areas with GW overexploitation.

4. Conclusions and discussion

In the present study, we quantified the relative contribution of climate and GW extraction to soil moisture trends using a LSM (CAS-LSM) that considers HWR based on four global meteorological forcing datasets. Comparing the simulations, the in-situ observational datasets, and the satellite-based ESA-CCI surface products demonstrated that the CAS-LSM is able to reliably represent soil moisture trends.

The main conclusions of this study are as follows. First, all four forcing data resulted in similar patterns of surface soil moisture, and have higher soil moisture than ESA-CCI. Results at the regional scale (Fig. 4) indicated that the uncertainty of the forcing data affected the simulated soil moisture. Therefore, the ensemble average results were used to reduce the uncertainty caused by the forcing data. Second, our results show a significant decreasing trend in surface and deep soil moisture over the 32-year period investigated. For the surface soil, GW extraction slowed the drying trend in drying areas and increased the wetting trend in wetting areas. This is because GW extraction is mainly used for irrigation as effective water input into the topsoil. While has opposite effect on deep soil when the hydrological connection between the aquifer and deep soil was weakened due to the extraction severely. Third, climate contributed 101.2% and 90.7% to global drying and wetting trends of surface soil moisture, while GW extraction had a relative weak effect on soil moisture (−1.2% and 9.3% for global drying and wetting, respectively). For deep soil, GW extraction contributed 1.37% and −3.21% to the drying and wetting trends. This is because there are limited areas that exploit GW. Regionally, GW extraction contributed more in regions with high water demand for irrigation, production, and human consumption. In typical water-use areas, including the North China Plain, Central US, and North India, GW extraction contributed more to the soil moisture trends than in the regions almost without GW extraction. In summary, climate change dominates the soil moisture trends, while GW extraction accelerates or decelerates soil moisture trends under climate change.

Our study demonstrated the effect of GW extraction on soil moisture. Future research should focus on developing strategies to adapt to climate change. At the same time, the effect of GW exploitation on regional soil moisture cannot be ignored. Over-exploitation weakens the hydraulic connection between soil and aquifer, which may affect root growth and development. Furthermore, GW extraction also impact atmosphere. Zeng et al. (2016b) found that the cooling caused by GW extraction in northern India weakened the Indian monsoon and its water vapor transport and the precipitation decreased. Therefore,

the development and utilization of water resources must consider the local ecological and atmospheric environment.

The mismatch of soil layers between the simulations and observations may affect the evaluation results. Also, our results indicate that it is necessary to consider human activities in LSMs, and improved descriptions of hydrological processes in LSMs are required. For example, GW extraction is assumed to be occur in the area it is consumed in. Moreover, meteorological forcing data can introduce uncertainty for simulation results. The precipitation data used in our study showed significant differences. The WFD precipitation evidently decreased (1.96 mm yr^{-1}), and the GSWP precipitation slightly decreased (0.16 mm yr^{-1}), while for CRU-NCEP and PRINCETON, precipitation slightly increased. Temperature varied similarly for all four forcing datasets (slightly increasing). The ensemble averaging method used in this study is not the optimum choice. However, considering that the purpose of this study was to explore the contribution of GW extraction to soil moisture trends, this simple averaging approach was reasonable. It is necessary to use a more appropriate averaging method to minimize the uncertainty caused by the forcing data in future work.

Future studies should focus on two aspects. First, GW extraction should be improved to reflect realistic levels of water consumption. The GW extraction scheme used in this study is a simple bottom-up representation, the irrigation demand is the water required to bring the soil moisture to saturation at each time step, which describes an extreme water requirement and significantly overestimates the actual irrigation water demand. Next work will focus on a more realistic definition of irrigation water demand, such as the demand based on the difference between the potential evapotranspiration and available water. Thus, simulations using the improved model would more accurately reflect hydrological effects and enhance water resource management. Second, since only the effect of HWR was discussed in this study, other human activities could also be considered. For instance, the association between soil moisture and land-cover change can be evaluated. Changes in land-surface cover affect the hydrothermal properties of the surface soil, which further affects soil moisture.

Code/Data availability. The model code and data are available upon request. Please contact Zhenghui Xie at zxie@lasg.iap.ac.cn

Author contribution. Longhuan Wang and Zhenghui Xie designed the research; Longhuan Wang performed the simulations, analyzed the data, and drafted the paper with contributions from all authors.

Competing interests. The authors declare that they have no conflict of interest.

Acknowledgements. This work was jointly supported by the National Natural Science Foundation of China (Grants 41830967), the National Key R&D Program of China (2018YFC1506602) and by the Key Research Program of Frontier Sciences, CAS (QYZDY-SSW-DQC012). The ESA CCI soil moisture dataset was downloaded from http://www.esa-soilmoisture-cci.org; the in-situ soil moisture observations were downloaded from http://www.geo.tuwien.ac.at/insitu/data_viewer/ISMN.php. We thank Yun Liu and two other anonymous reviewers for the helpful comments that improved the manuscript.

References

Albergel, C., Rüdiger, C., Pellarin, T., Calvet, J. C., Fritz, N., Froissard, F., Suquia, D., Petitpa, A., Piguet, B., and Martin, E.: From near-surface to root-zone soil moisture using an exponential filter: An assessment of the method based on in-situ observations and model simulations. Hydrology and Earth System Sciences, 12(6), 1323–1337, 2008.

Albergel, C., de Rosnay, P., Gruhier, C., Muñoz-Sabater, J., Hasenauer, S., Isaksen, L., Kerr, Y., and Wagner, W.: Evaluation of remotely sensed and modelled soil moisture products using global ground-based in-situ observations, Remote Sens. Environ, 118, 215–226, 2012.

Albergel, C., Dorigo, W., Balsamo, G., Muñoz-Sabater, J., De Rosnay, P., and Isaksen, L., Brocca, L., de Jeu, R., and Wagner, W.: Monitoring multi-decadal satellite earth observation of soil moisture products through land surface reanalyses, Remote Sens. Environ, 138, 77-89, 2013.

Berg, Aaron A.: Impact of bias correction to reanalysis products on simulations of North American soil moisture and hydrological fluxes, Journal of Geophysical Research, 108(D16):ACL 2-1-ACL 2-15, 2003.

Best, M. J., Pryor, M., Clark, D. B., Rooney, G. G., Essery, R. L. H., Ménard, C. B., Edwards, J. M., Hendry, M. A., Porson, A., Gedney, N., Mercado, L. M., Sitch, S., Blyth, E., Boucher, O., Cox, P.

449 M., Grimmond, C. S. B., and Harding, R.J.: The Joint UK Land Environment Simulator (JULES),
450 model description– Part 1: energy and water fluxes, Geosci. Model Dev, 4, 677–699, 2011.
451 Cai, W., Cowan, T., Briggs, P., and Raupach, M.: Rising temperature depletes soil moisture and
452 exacerbates severe drought conditions across southeast Australia, Geophysical Research Letters,
453 36(21), 272-277, 2009.
454 Calvet, J. C., Fritz, N., Froissard, F., Suquia, D., Petitpa, A., and Piguet, B.: In-situ soil moisture
455 observations for the CAL/VAL of SMOS: The SMOSMANIA network, Proceedings of the IEEE
456 International Geoscience and Remote Sensing Symposium (IGARSS), 2008.
457 Cappelaere, B., Descroix, L., Lebel, T., Boulain, N., Ramier, D., Laurent, J.-P., Favreau, G., Boubkraoui,
458 S., Boucher, M., Moussa, I. B., Chaffard, V., Hiernaux, P., Issoufou, H. B. A., Le Breton, E.,
459 Mamadou, I., Nazoumou, Y., Oï, M., Ottlé, C. and Quantin, G.: The AMMA-CATCH experiment
460 in the cultivated Sahelian area of south-west Niger - Investigating water cycle response to a
461 fluctuating climate and changing environment, Journal of Hydrology, 375(1-2), 34–51, 2009.
462 Cheng, S. J., and Huang, J. P.: Enhanced soil moisture drying in transitional regions under a warming
463 climate, Journal of Geophysical Research: Atmospheres, 121(6):2542-2555, 2016.
464 Coe, M. T., and Foley, J. A.: Human and natural impacts on the water resources of the lake chad basin,
465 Journal of Geophysical Research: Atmospheres, 106(D4), 3349-3356, 2001.
466 Compo, G. P., Whitaker, J. S., Sardeshmukh, P. D., Matsui, N., Allan, R. J., Yin, X., Gleason, B. E.,
467 Vose, R. S., Rutledge, G., Bessemoulin, P., Brönnimann, S., Brunet, M., Crouthamel, R. I., Grant,
468 A. N., Groisman, P. Y., Jones, P. D., Kruk, M. C., Kruger, A. C., Marshall, G. J., Maugeri, M.,
469 Mok, H. Y., Nordli, Ø., Ross, T. F., Trigo, R. M., Wang, X. L., Woodruff, S. D., and Worley, S.
470 J.: The Twentieth Century Reanalysis Project, Quart. J. Roy. Meteor. Soc., 137, 1–28, 2011.

471 Dai, A. G.: Characteristics and trends in various forms of the palmer drought severity index during
472 1900–2008, Journal of Geophysical Research: Atmospheres, 116(D12), 2011.
473 Dai, A. G.: Increasing drought under global warming in observations and models, Nature Climate
474 Change, 3(1), 52-58, 2013.
475 de Rosnay, P. D., Gruhier, C., Timouk, F., Baup, F., Mougin, E., and Hiernaux, P., Kergoat, L., and
476 LeDantec, V.: Multi-scale soil moisture measurements at the Gourma meso-scale site in mali.
477 Journal of Hydrology (Amsterdam), 375(1-2), 241-252, 2009.
478 Dorigo, W.A., Wagner, W., Hohensinn, R., Hahn, S., Paulik, C., Xaver, A., Gruber, A., Drusch, M.,
479 Mecklenburg, S., van Oevelen, P., Robock, A., and Jackson, T.: The International Soil Moisture
480 Network: A data hosting facility for global in-situ soil moisture measurements, Hydrology and
481 Earth System Sciences, 15 (5), 1675-1698, 2011.
482 Dorigo, W.A., Jeu, R.D., Chung, D., Parinussa, R., Liu, Y., Wagner, W., and Fernández-Prieto, D.:
483 Evaluating global trends (1988–2010) in harmonized multi-satellite surface soil moisture,
484 Geophysical Research Letters, 39(18), 18405, 2012.
485 Dorigo, W. A. , Xaver, A. , Vreugdenhil, M. , Gruber, A. , Hegyiová, A., Sanchis-Dufau, A. D., Zamojski,
486 D., Cordes, C., Wagner, W., and Drush, M.: Global automated quality control of in-situ soil
487 moisture data from the international soil moisture network, Vadose Zone Journal, 12(3), 918-924,
488 2013.
489 Döll, P., Fiedler, K. and Zhang, J.: Global-scale analysis of river flow alterations due to water
490 withdrawals and reservoirs, Hydrol. Earth Syst. Sci. 13 2413–32, 2009.

491 Douville, H., Ribes, A., Decharme, B., Alkama, R. and Sheffield, J. Anthropogenic influence on
492 multidecadal changes in reconstructed global evapotranspiration, Nature Clim. Change 3, 59–62,
493 2013.
494 Feng, H. H., and Liu, Y. B.: Trajectory based detection of forest-change impacts on surface soil moisture
495 at a basin scale [Poyang Lake Basin, China], J. Hydrol. 514, 337–346, 2014.
496 Feng, H. H., and Zhang, M. Y.: Global land moisture trends: drier in dry and wetter in wet over land,
497 Sci. Rep. 5, 18018; doi: 10.1038/srep18018, 2015.
498 Feng, H. H.: Individual contributions of climate and vegetation change to soil moisture trends across
499 multiple spatial scales, Sci. Rep. 6, 32782; doi: 10.1038/srep32782, 2016.
500 Guo, Z., Dirmeyer, P., Zeng, Z. H., Gao, X., and Zhao, M.: Evaluation of the Second Global Soil
501 Wetness Project soil moisture simulations: 2. Sensitivity to external meteorological forcing, J.
502 Geophys. Res., 111, D22S03, https://doi.org/10.1029/2006JD007845, 2006.
503 Haddeland, I., Clark, D. B., Franssen, W., Ludwig, F., Voß, F., Arnell, N. W., Bertrand, N., Best, M.,
504 Folwell, S., Gerten, D., Gomes, S., Gosling, S. N., Hagemann, S., Hanasaki, N., Harding, R.,
505 Heinke, J., Kabat, P., Koirala, S., Oki, T., Polcher, J., Stacke, T., Viterbo, P., Weedon, G. P., and
506 Yeh, P.: Multimodel Estimate of the Global Terrestrial Water Balance: Setup and First Results,
507 Journal of Hydrometeorology., 12, 869–884, 2011.
508 Hulme, M.: Rainfall changes in africa: 1931–1960 to 1961–1990, International Journal of Climatology,
509 12(7), 685-699, 1992.
510 Hurtt, G. C., Chini, L. P., Frolking, S., Betts, R. A., Feddema, J., Fischer, G., Fisk, J. P., Hibbard, K.,
511 Houghton, R. A., Janetos, A., Jones, C. D., Kindermann, G., Kinoshita, T., Goldewijk, K. K., Riahi,
512 K., Shevliakova, E., Smith, S., Stehfest, E., Thomson, A., Thornton, P., van Vuuren, D. P., and

513 Wang, Y. P.: Harmonization of land-use scenarios for the period 1500–2100: 600 years of global
514 gridded annual land-use transitions, wood harvest, and resulting secondary lands, Climatic Change,
515 109(1-2), 117, 2011.
516 Jia, B. H., Liu, J. G., Xie Z. H., and Shi, C. X.: Interannual variations and trends in remotely sensed and
517 modeled soil moisture in China, Journal of Hydrometeorology. 19, 831-847, 2018.
518 Kim, H., Watanabe, S., Chang, E-.C., Yoshimura, K., Compo, G. P., Hirabayashi, Y., Famiglietti, J.,
519 and Oki, T.: A century-long global surface meteorology for offline terrestrial simulations, in
520 preparation, 2016.
521 Kowalczyk, E.A., Wang, Y.P., Law, R.M., Davies, H.L., McGregor, J.L., and Abramowitz, G.: The
522 CSIRO Atmosphere Biosphere Land Exchange (CABLE) model for use in climate models and as
523 an offline model. CSIRO Marine and Atmospheric Research Paper 013:
524 http://www.cmar.csiro.au/e-print/open/kowalczykea_2006a.pdf, 2006.
525 Kottek, M., Grieser, J., Beck, C., Rudolf, B. and Rubel, F.: World Map of the Köppen-Geiger climate
526 classification updated, Meteorol. Z15, 259–263, 2006.
527 Lawrence, D. M., Oleson, K. W., Flanner, M. G., Thorton, P. E., Swenson, S. C., Lawrence, P. J., Zeng,
528 X. B., Yand, Z. L., and Levis, S.: Parameterization improvements and functional and structural
529 advances in version 4 of the Community Land Model, Journal of Advances in Modeling Earth
530 Systems, 3, M03001, 2011.
531 L' Hôte Y, Mahé G, Somé B, and Triboulet JP.: Analysis of a sahelian annual rainfall index from 1896
532 to 2000; the drought continues, International Association of Scientific Hydrology Bulletin, 47(4),
533 10, 2002.

534 Li, M., Ma, Z. G., and Niu, G. Y.: Modeling spatial and temporal variations in soil moisture in China.
535 Chin. Sci. Bull., 56, 1809–1820, https://doi.org/10.1007/s11434-011-4493-0, 2011.
536 Marczewski, W., Slominski, J., Slominska, E., Usowicz, B., Usowicz, J., Romanov, S., Maryskevych,
537 O., Nastula, J., and Zawadzki, J.: Strategies for validating and directions for employing SMOS
538 data, in the Cal-Val project SWEX (3275) for wetlands. Hydrology and Earth System Sciences
539 Discussions, 7, 7007–7057, 2010.
540 Min, S-K., Zhang, X. B., Zwiers, F. W. and Hegerl, G. C.: Human contribution to more-intense
541 precipitation extremes, Nature 470, 378–382, 2011.
542 Mougin, E., Hiernaux, P., Kergoat, L., Grippa, M., de Rosnay, P., Timouk, F., Le Dantec, V., Demarez,
543 V., Lavenu, F., Arjounin, M., Lebel, T., Soumaguel, N., Ceschia, E., Mougenot, B., Baup, F.,
544 Frappart, F., Frison, P. L., Gardelle, J., Gruhier, C., Jarlan, L., Mangiarotti, S., Sanou, B., Tracol,
545 Y., Guichard, F., Trichon, V., Diarra, L., Soumaré, A., Koité, M., Dembélé, F., Lloyd, C., Hanan,
546 N. P., Damesin, C., Delon, C., Serca, D., Galy-Lacaux, C., Seghieri, J., Becerra, S., Dia, H.,
547 Gangneron, F., and Mazzega, P.: The AMMA-CATCH Gourma observatory site in Mali: Relating
548 climatic variations to changes in vegetation, surface hydrology, fluxes and natural resources.
549 Journal of Hydrology, 375, 14–33, 2009.
550 Oleson, K: Technical description of version 4.5 of the Community Land Model (CLM), NCAR Tech.
551 Note NCAR/TN-503+ STR, Boulder, Colo., 420pp, 2013.
552 Omole, D. O.: Sustainable groundwater exploitation in Nigeria. J. Water Resour. Ocean Sci., 2, 9–14,
553 doi:10.11648/j.wros.20130202.11, 2013.

554 Pellarin, T., Laurent, J. P., Cappelaere, B., Decharme, B., Descroix, L., and Ramier, D.: Hydrological
555 modelling and associated microwave emission of a semi-arid region in South-western Niger.
556 Journal of Hydrology, 375, 262–272, 2009.
557 Robock, A., Vinnikov, K. Y., Srinivasan, G., Entin, J. K., Hollinger, S. E., Speranskaya, N. A., Liu, S.
558 X., and Namkhai, A.: The Global Soil Moisture Data Bank, Bull. Amer. Meteor. Soci., 81, 1281-
559 1299, 2000.
560 Robock, A., Mu, M., Vinnikov, K., Trofimova, I. V., and Adamenko T. I.: Forty-five years of observed
561 soil moisture in the Ukraine: No summer desiccation (yet), Geophys. Res. Lett., 32, L03401,
562 doi:10.1029/2004GL021914, 2005.
563 Rodell, M., I. Velicogna, and J. S. Famiglietti.: Satellite-based estimates of groundwater depletion in
564 India, Nature, 460, 999 –1002, doi:10.1038/nature08238, 2009.
565 Siebert, S., Döll, P., Hoogeveen, J. , Faures, J. M., Frenken, K., and Feick, S.: Development and
566 validation of the global map of irrigation areas, Hydrology and Earth System Sciences, 9, 535–547,
567 2005.
568 Sen, P. K.: Estimates of the regression coefficient based on Kendall's tau, J. Amer. Stat. Assoc., 63,
569 1379–1389, 1968.
570 Seneviratne, S., Corti, T., Davin, E., Hirschi, M., Jaeger, E., Lehner, I., Orlowsky, B., and Teuling, A.:
571 Investigating soil moisture–climate interactions in a changing climate: A review, Earth-Sci. Rev.,
572 99, 125–161, 2010.
573 Sheffield, J. , Goteti, G. , and Wood, E. F.: Development of a 50-year high-resolution global dataset of
574 meteorological forcings for land surface modeling, J. Climate, 19(13), 3088--3111, 2006.

575 Smith, A. B., Walker, J. P., Western, A. W., Young, R. I., Ellett, K. M., Pipunic, R. C., Grayson, R. B.,
576 Siriwardena, L., Chiew, F. H. B., and Richter, H.: The Murrumbidgee soil moisture monitoring
577 network dataset. Water Resources Research, 48(7), 7701, 2012.
578 Taylor, and Karl, E.: Summarizing multiple aspects of model performance in a single diagram, Journal
579 of Geophysical Research, 106(D7):7183, 2001.
580 Van Den Hurk, B., Best, M., Dirmeyer, P., Pitman, A., Polcher, J., and Santanello, J.: Acceleration of
581 Land Surface Model Development over a Decade of Glass, Bull. Amer. Meteor. Soci., 92, 1593–
582 1600. doi:10.1175/BAMS-D-11-00007.1, 2011.
583 Van Den Hurk, B., Kim, H. J., Krinner, G., Seneviratne, S.I., Derksen, C., Oki, T., Douville, H., Colin,
584 J., Ducharne, A., Cheruy, F., Viovy, N., Puma, M.J., Wada, Y., Li, W., Jia, B. H., Alessandri, A.,
585 Lawrence, D.M., Weedon G.P., Ellis, R., Hagemann, S., Mao, J., Flanner, M.G., Zampieri, M.,
586 Materia, S., Law, R.M., Sheffield, J.: LS3MIP (V1.0) contribution to CMIP6: The Land Surface,
587 Snow and Soil moisture Model Intercomparison Project – aims, setup and expected outcome,
588 Geosci. Model Dev., 9, 2809–2832, 2016.
589 Viovy, N., and Ciais, P.: A combined dataset for ecosystem modelling:
590 http://esgf.extra.cea.fr/thredds/catalog/store/ p529viov/cruncep/catalog.html, last access: 1 August
591 2016, 2009.
592 Wada, Y., Van Beek, L. P. H., Wanders, N., and Bierkens, M. F. P.: Human water consumption
593 intensifies hydrological drought worldwide, Environmental Research Letters, 2013,
594 8(3):034036,2013.
595 Wada, Y., L. P. H. van Beek, C. M. van Kempen, J. W. T. M. Reckman, S. Vasak, and M. F. P. Bierkens.:
596 Global depletion of groundwater resources, Geophys. Res. Lett., 37, L20402, 2010.

Wagner, W., Lemoine, G., and Rott, H.: A method for estimating soil moisture from ERS scatterometer and soil data, Remote Sens. Environ, 70(2), 191-207, 1999.

Wang, A. H., and Zeng, X. B.: Sensitivities of terrestrial water cycle simulations to the variations of precipitation and air temperature in China, J. Geophys. Res: Atmospheres, 2011, 116(D2) , 2011.

Weedon, G. P., Balsamo, G., Bellouin, N., Gomes, S., Best, M. J., and Viterbo, P.: The WFDEI meteorological forcing dataset: WATCH Forcing Data methodology applied to ERAInterim reanalysis data, Water Resour. Res., 50, 7505–7514, 2014.

Wei, J., Dirmeyer, P. A., and Guo, Z.: Sensitivities of soil wetness simulation to uncertainties in precipitation and radiation, Geophys. Res. Lett., 35, L15703. doi:10.1029/2008GL034494, 2008.

Wentz, F. J., Ricciardulli, L., Hilburn, K. and Mears, C.: How Much More Rain Will Global Warming Bring? Science 13, 233–235, 2007.

Wisser, D., Fekete, B. M., Vörösmarty, C. J. and Schumann, A. H.: Reconstructing 20th century global hydrography: acontribution to the global terrestrial network-hydrology (GTNH), Hydrol. Earth Syst. Sci., 14 1–24, 2010.

Wu, B., Zheng, Y., Tian, Y., Yao, Y. Y., Han, F., Liu, J., Zheng, C. M.: Systematic assessment of the uncertainty in integrated surface water–groundwater modeling based on the probabilistic collocation method. Water Resour. Res., 50, 5848–5865, doi:10.1002/2014WR015366, 2014.

Xie Z. H., Liu S., Zeng Y. Y., Gao J. Q., Qin P. H., Jia, B. H., Xie, J. B., Liu, B., Li, R. C., Wang, Y., and Wang, L. H.: A high-resolution land model with groundwater lateral flow, water use and soil freeze-thaw front dynamics and its applications in an endorheic basin, J. Geophys. Res.-Atmos., 123, 7204-7222. https://doi.org/10.1029/2018JD028369, 2018.

618 Yin, Z., Ottlé, C., Ciais, P., Guimberteau, M., Wang, X. H., Zhu, D., Maignan, F., Peng, S. S., Piao, S.
619 L., Polcher, J., Zhou, F., Kim, H., and other China-Trend-Stream project members.: Evaluation of
620 ORCHIDEE-MICT-simulated soil moisture over China and impacts of different atmospheric
621 forcing data, Hydrol. Earth Syst. Sci., 22, 5463–5484, https://doi.org/10.5194/hess-22-5463-2018,
622 2018.
623 Yu, Y., Xie, Z. H., and Zeng, X. B.: Impacts of modified Richards equation on RegCM4 regional climate
624 modeling over East Asia, J. Geophys. Res.-Atmos., 119, 12642–12659, doi:10.1002/2014jd021872,
625 2014.
626 Zeng, Y. Y., Xie, Z. H., and Liu, S.: Seasonal effects of irrigation on land-atmosphere latent heat,
627 sensible heat, and carbon fluxes in semiarid basin, Earth System Dynamics, 8(1), 113–127, 2017.
628 Zeng, Y. Y., Xie, Z. H., Yu, Y., Liu, S., Wang, L. Y., Zou, J., Qin, P. H., and Jia, B. H.: Effects of
629 anthropogenic water regulation and groundwater lateral flow on land processes, Journal of
630 Advances in Modeling Earth Systems, 8(3), 1106–1131, 2016a.
631 Zeng, Y. Y., Xie, Z. H., and Zou, J.: Hydrologic and climatic responses to global anthropogenic
632 groundwater extraction, J. Climate, 30. 10.1175/JCLI-D-16-0209.1, 2016b.
633 Zhan, X., Zheng, W., Fang, L., Liu, J., Hain, C., Yin, J., and Ek, M.: A preliminary assessment of the
634 impact of SMAP soil moisture on numerical weather forecasts from GFS and NUWRF models,
635 IGARSS 2016 - 2016 IEEE International Geoscience and Remote Sensing Symposium, IEEE,
636 5229–5232, 2016.
637 Zou, J., Xie, Z. H., Zhan, C. S., Qin, P. H., Sun, Q., Jia, B. H., and Xia, J.: Effects of anthropogenic
638 groundwater exploitation on land surface processes: A case study of the Haihe River Basin,
639 northern China. J. Hydrol., 524, 625–641, doi:10.1016/j.jhydrol.2015.03.026, 2015.

640 Zou, J., Xie, Z. H., Yu, Y., Zhan, C. S., and Sun, Q.: Climatic responses to anthropogenic groundwater
641 exploitation: A case study of the Haihe River Basin, northern China, Climate Dyn., 42 , 2125–2145,
642 2014.

643 Tables

644 **Table 1.** General information of the meteorological forcing datasets

Data	Spatial	Interval	Time period	Source
GSWP	0.5°	3-hourly	1901–2012	[Kim et al., 2016]
WFD/WFDEI	0.5°	3-hourly	1901–2000/1979–2014	[Haddeland et al., 2011; Weedon at al., 2014]
CRU-NCEP	0.5°	6-hourly	1901–2010	[Viovy and Ciais, 2009]
PRINCETON	0.5°	3-hourly	1901–2012	[Sheffield et al., 2006]

645

646

647 **Table 2.** Details for the stations used in this study.

Continent	Network name	Country	Number of sites used	Depths (m)	Corresponding simulated soil layer	References
Africa	AMMA-CATCH	Benin, Niger	4	0.05;0.2,0.4	3,5,6	Cappelaere et al. (2009); de Rosnay et al. (2009); Mougin et al. (2009); Pellarin et al. (2009)
Australia	OZNET	Australia	8	0–0.3;0.3–0.6; 0.6–0.9	1–5;6–7;7	Smith et al. (2012)
Europe	SMOSMANIA, ORACLE, SWEX_POLAND	France, Poland	20	0.05;0.1; 0.2;0.3	3;4;5;6	Albergel et al. (2008); Calvet et al. (2008); https://bdoh.irstea.fr/ORACLE/ Marczewski et al. (2010)
North America	SNOTEL, SCAN	US	82	0.05;0.2;0.5	3;5;6–7	http://www.wcc.nrcs.usda.gov/snow/ http://www.wcc.nrcs.usda.gov/scan/
Asia	IIT_KANPUR	India	1	0.1;0.25; 0.5;0.8	4;5;6–7;7	http://www.iitk.ac.in/
Asia	CHINA	China	40	0–0.1;0.1–0.2; 0.2–0.3;0.3–0.5	1–3;4;5;7	Robock et al. (2000)

Asia	MONGOLIA	Mongolia	28	0–0.1,0.1–0.2, 0.2–0.3	1–3;4;5	Robock et al. (2000)
Asia	RUSWET-GRASS	Former Soviet Union	30	0–0.1,0–1	1–3;1–8	Robock et al.(2000)

650 **Table 3.** Trends in NEW simulated surface soil moisture and precipitation and
651 temperature of forcing data. * = $p < 0.05$.

NEW	SM ($m^3m^{-3}yr^{-1}$)	Pre ($mmyr^{-1}$)	Tem ($°C\ yr^{-1}$)
GSWP	*−0.89e−4	−0.16	*0.017
CRU-NCEP	*−0.97e−4	−0.27	*0.017
PRINCETON	−0.65e−4	−0.008	*0.017
WFD	*−0.15e−3	*−1.96	*0.019

652
653

Figures

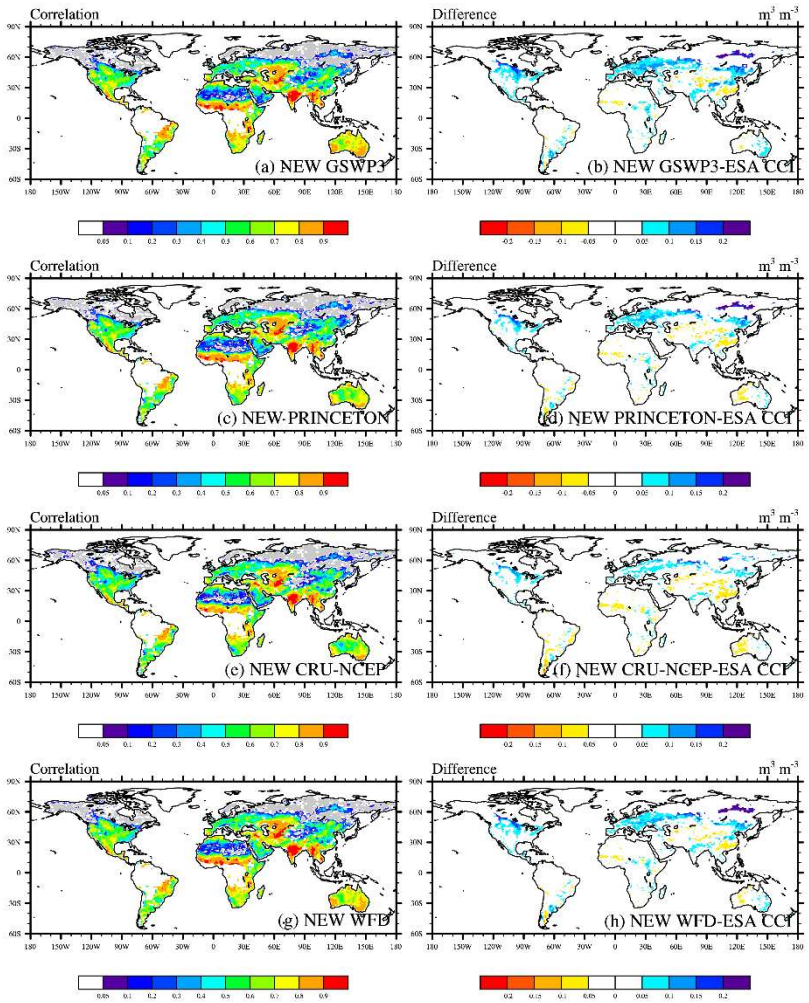

Figure 1. Correlation coefficients (a, c, e, g) and differences of spatial patterns (b, d, f, h) of the ESA CCI soil moisture and the corresponding simulated top 10 cm soil moisture from 1979–2010. Gray pixels indicate no correlation and negative correlation.

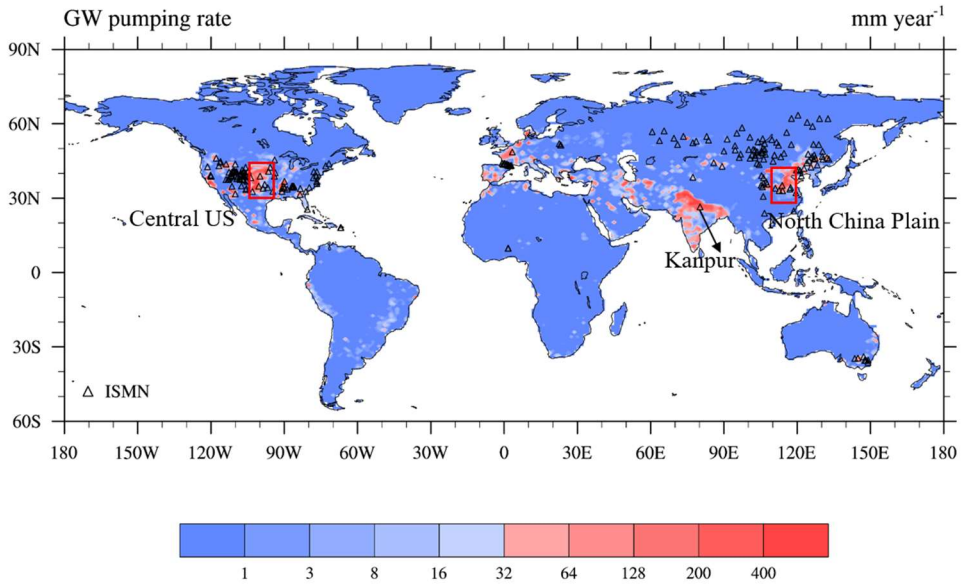

Figure 2. Distribution of soil moisture stations and three subregions. Seven stations on the North China Plain, 15 in central US, and one in Kanpur of North India). The background is the groundwater (GW) extraction rate.

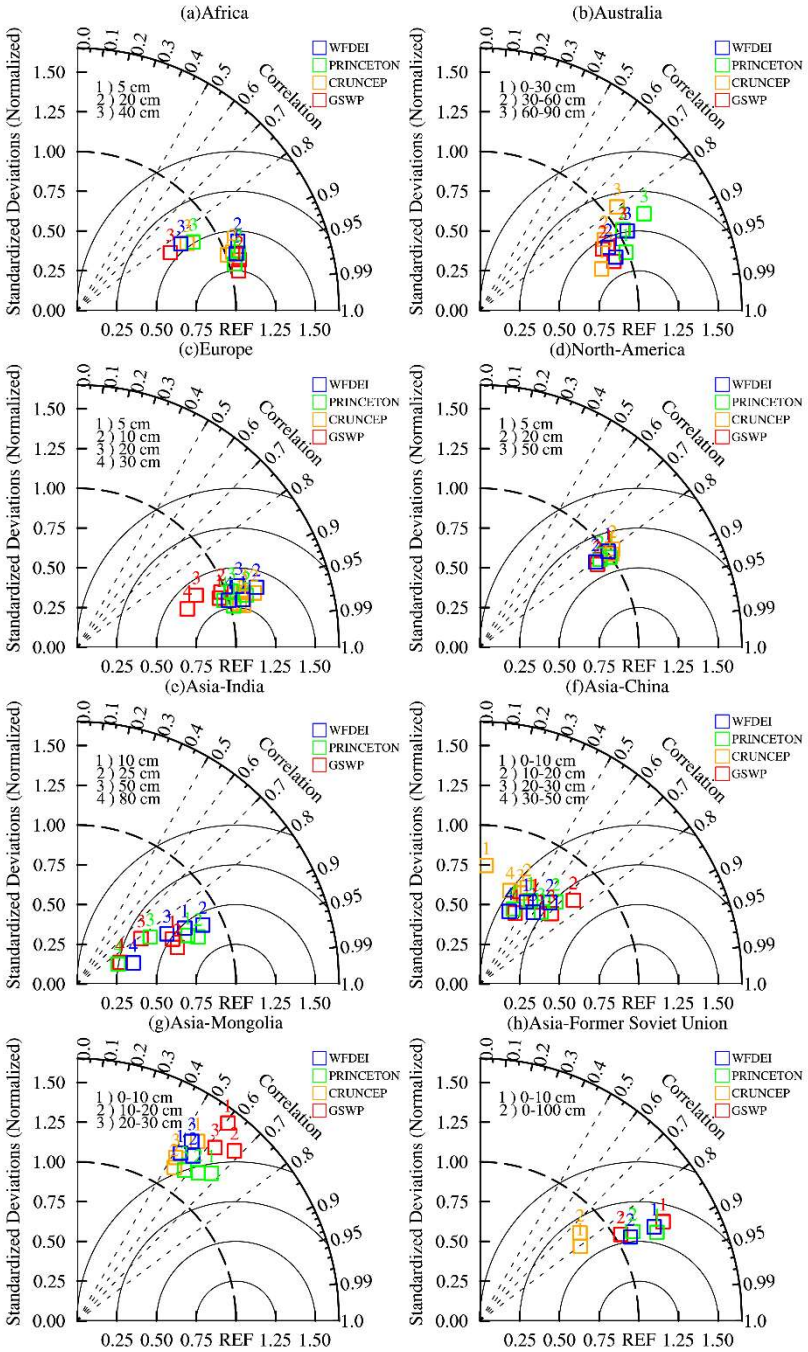

665

666 **Figure 3.** Taylor diagrams illustrating the comparisons among GSWP, CRUNCEP, PRINCETON, WFDEI, and in-
667 situ observation data.

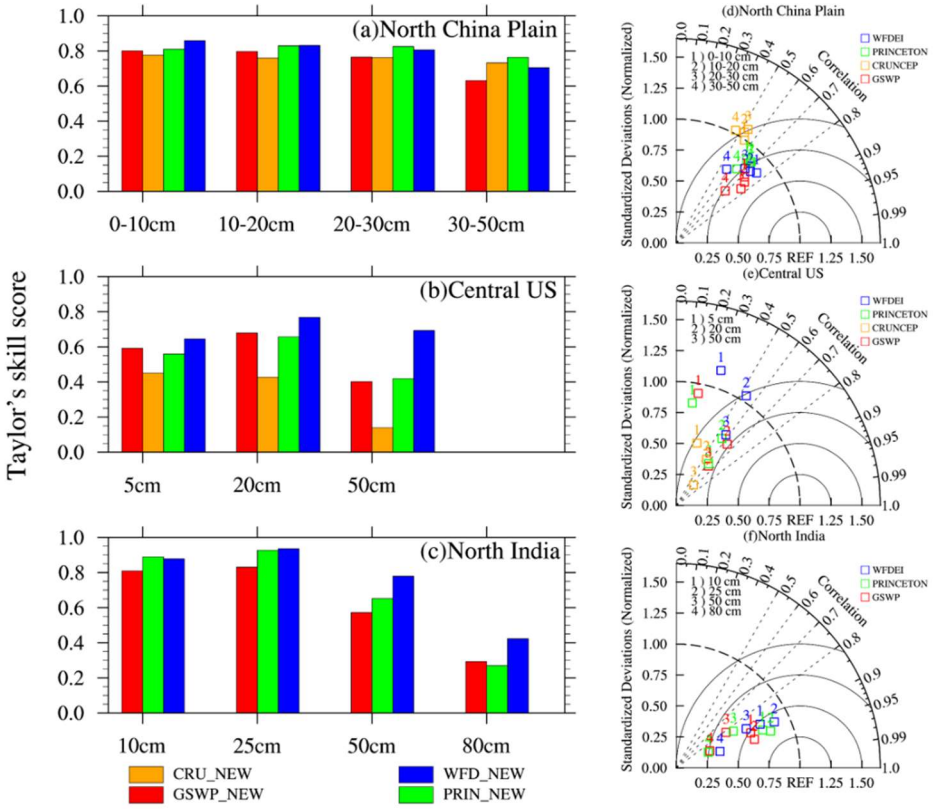

668

669 **Figure 4.** Taylor's skill scores and Taylor diagrams illustrating the comparisons among GSWP, CRUNCEP,
670 PRINCETON, WFDEI, and in-situ observations. (a, d) North China Plain; (b, e) Colorado of Central US; (c, f) North
671 India. The azimuthal angle represents the correlation coefficient, and radial distance is the standard deviation
672 normalized to observations.

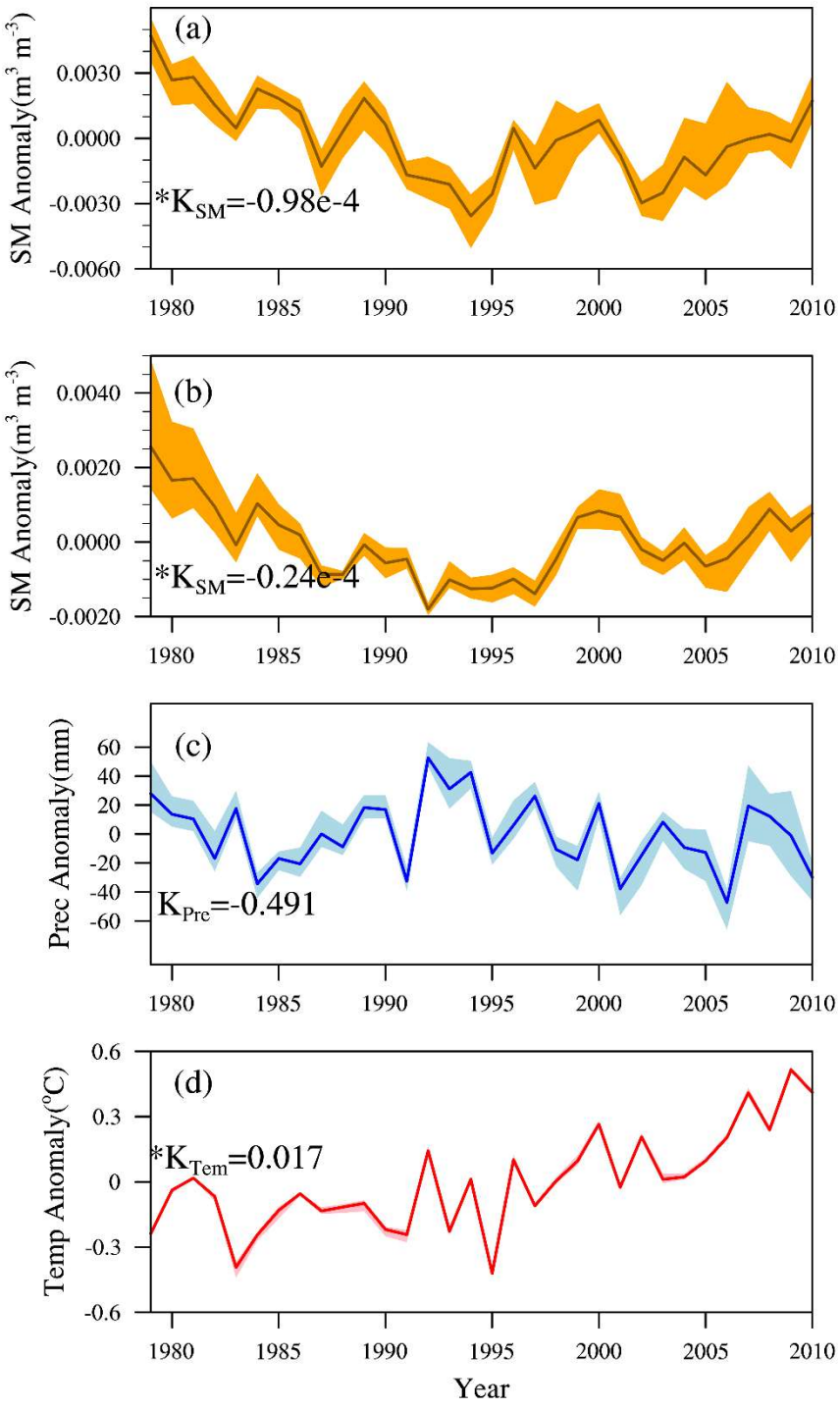

673

674 **Figure 5.** Annual mean of (a) surface soil moisture, (b) deep soil moisture, (c) precipitation, and (d) temperature
675 averaged globally from 1979–2010. * = $p < 0.05$.

676

677

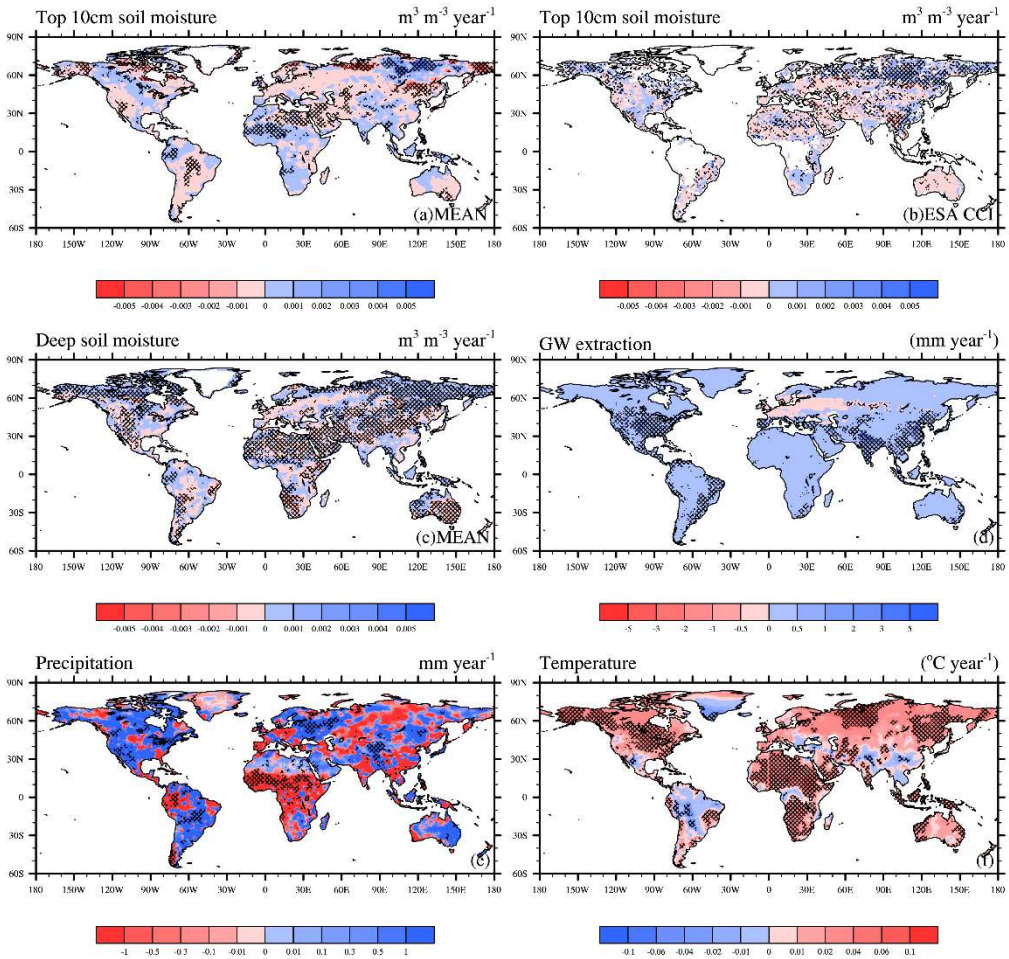

678

679 **Figure 6.** The spatial distribution of linear trends for (a) simulated surface soil moisture ($m^3 m^{-3} yr^{-1}$) and (b) surface
680 soil moisture from ESA CCI ($m^3 m^{-3} yr^{-1}$), (c) simulated deep soil moisture ($m^3 m^{-3} yr^{-1}$), (d) groundwater extraction
681 (mm yr^{-1}), (e) precipitation (mm yr^{-1}), (f)temperature (°C yr^{-1}). The shaded areas represent grids with statistically
682 significant trends ($p < 0.05$).

683

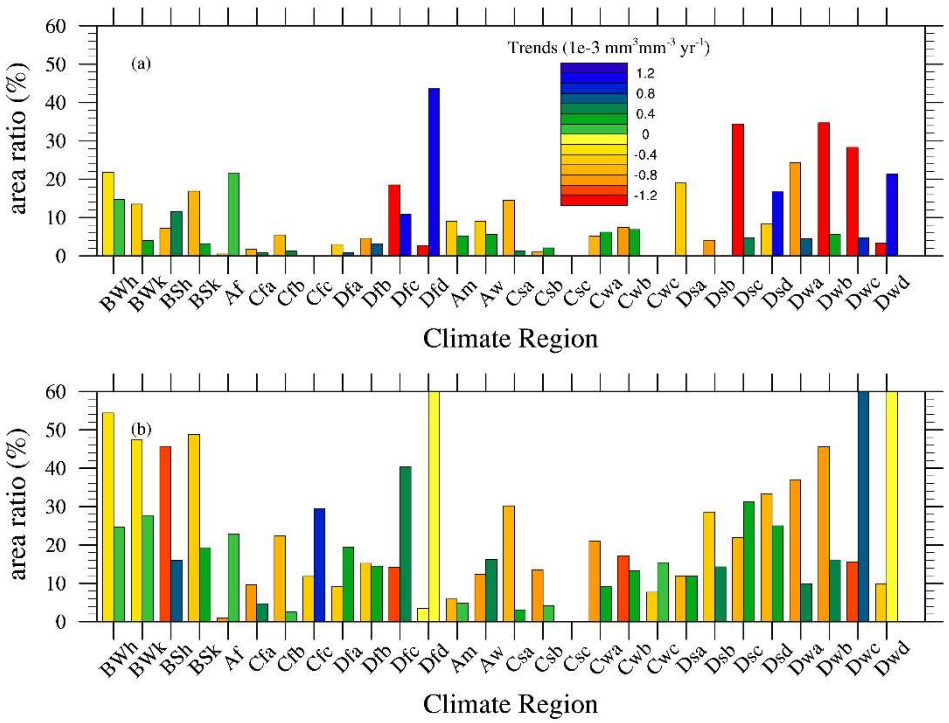

684

685 **Figure 7.** Statistics of the soil moisture trends. (a, b) The ratio of surface and deep soil moisture to wet and dry for
686 28 Köppen-Geiger climate types. For each type, the left bar is the drying ratio and the right bar is the wetting ratio.

687

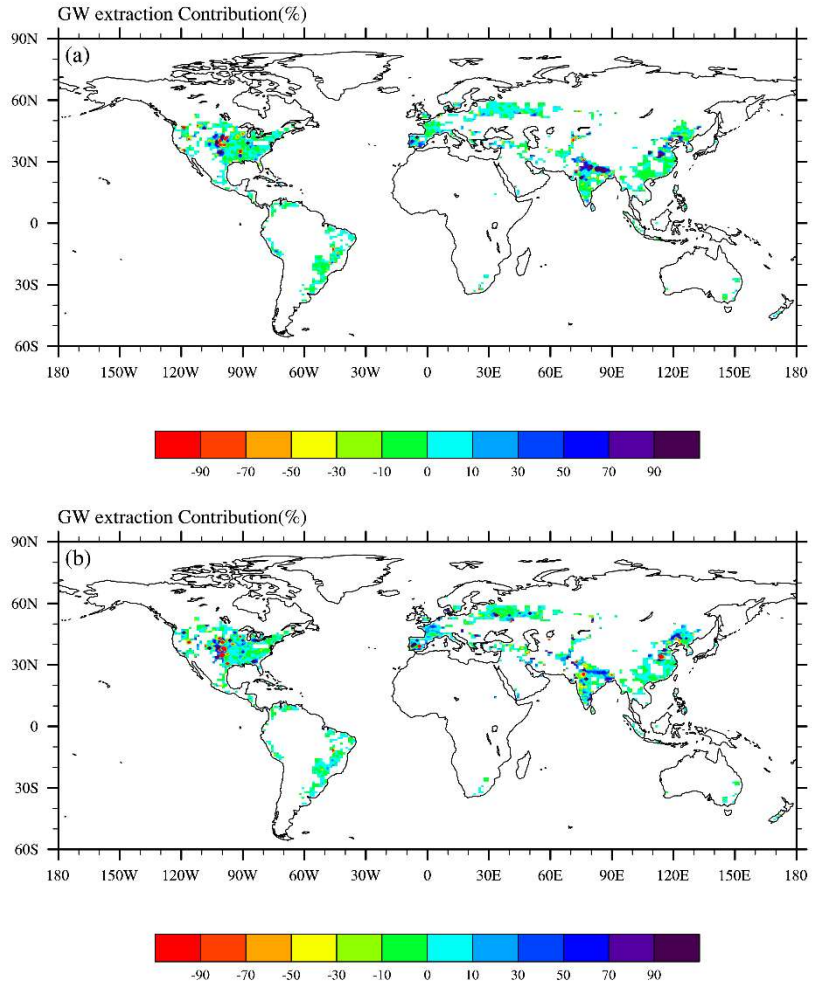

Figure 8. The relative contribution of groundwater extraction to (a) surface and (b) deep soil moisture trends (%).

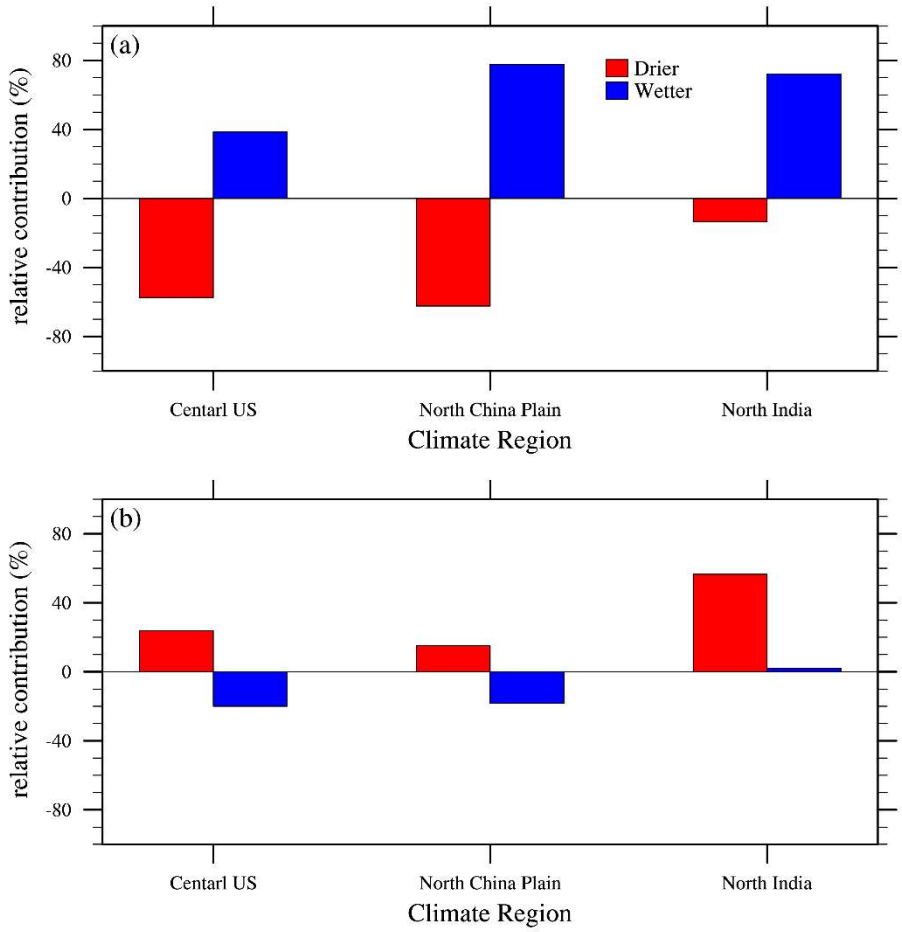

693

694 **Figure 9.** The relative contribution of GW extraction to regional (a) surface, (b) deep soil moisture trends (%). North
695 China Plain (34°–40° N, 110°–120° E), northern India (23°–33° N, 68°–78° E), central US (33°–42° N, 97°–105°
696 W).